# Dynamics of Langmuir wave decay in two dimensions

L. F. Ziebell, R. Gaelzer, and P. H. Yoon

Citation: Physics of Plasmas **15**, 032303 (2008); doi: 10.1063/1.2844740
View online: http://dx.doi.org/10.1063/1.2844740
View Table of Contents: http://scitation.aip.org/content/aip/journal/pop/15/3?ver=pdfcov
Published by the AIP Publishing



# Dynamics of Langmuir wave decay in two dimensions

L. F. Ziebell,[1,a)] R. Gaelzer,[2,b)] and P. H. Yoon[3,c)]
[1]*Instituto de Física, UFRGS, Porto Alegre, RS, Brazil*
[2]*Instituto de Física e Matemática, UFPel, Pelotas, RS, Brazil*
[3]*IPST, University of Maryland, College Park, Maryland 20742, USA*

(Received 17 July 2007; accepted 13 January 2008; published online 4 March 2008)

The present paper reports on the first two-dimensional (2D) self-consistent solution of weak turbulence equations describing the evolution of electron-beam-plasma interaction in which quasilinear as well as nonlinear three-wave decay processes are taken into account. It is found that the 2D Langmuir wave decay processes lead to the formation of a quasicircular ring spectrum in wave number space. It is also seen that the 2D ring-spectrum of Langmuir turbulence leads to a tendency to isotropic heating of the electrons. These findings contain some important ramifications. First, in the literature, isotropization of energetic electrons, detected in the solar wind for instance, is usually attributed to pitch-angle scattering. The present finding constitutes an alternative mechanism, whose efficiency for other parametric regimes has to be investigated. Second, when projected onto the one-dimensional (1D) space, the 2D ring spectrum may give a false impression of Langmuir waves inverse cascading to longer wavelength regime, when in reality, the wavelength of the turbulence does not change at all but only the wave propagation angle changes. Although the present analysis excludes the induced scattering, which is another process potentially responsible for the inverse cascade, the present finding at least calls for an investigation into the relative efficacy of the inverse-cascading process in 1D vs 2D. © *2008 American Institute of Physics*.
[DOI: 10.1063/1.2844740]

## I. INTRODUCTION

The study of electron beam-plasma interaction has many applications in laboratory and space plasmas. The beam-plasma interaction is characterized by Langmuir turbulence and emission of electromagnetic radiation. The best example of beam-plasma interaction in nature may be the solar type II and III radio bursts.[1–3] Energetic electrons in the source regions of these radio bursts excite Langmuir turbulence by bump-on-tail instability. Nonlinear mode coupling (decay and scattering) then converts part of the wave energy in the Langmuir turbulence to electromagnetic radiation. This so-called plasma emission scenario involves merging of the primary and backscattered Langmuir ($L$) waves into electromagnetic (EM) radiation at twice the plasma frequency, and/or the decay of $L$ waves into a transverse wave at the fundamental plasma frequency and an ion-sound ($S$) wave. Despite the fact that this standard scenario is discussed much in the literature, the detailed quantitative analysis based upon actual numerical solutions of the weak turbulence equation is not available in the literature. One of the major difficulties is that the simplifying assumption of one-dimensionality (1D) cannot be made for the radiation generation problem. Because of this, for a detailed numerical study of EM radiation involving decay/coalescence of $L$ and $S$ waves, simple model two-dimensional (2D) spectra of the primary and backward-traveling Langmuir turbulence have been assumed in the literature.[4–7]

The beam-plasma interaction problem is an ideal natural phenomena against which various features of nonlinear plasma turbulence theories can be tested. For instance, it is commonly assumed that the beam-generated Langmuir turbulence may suffer an inverse cascade so that over a long time period, long-wavelength undamped Langmuir waves can accumulate (the so-called "Langmuir condensation" phenomenon). As a mechanism to check the unlimited growth of the condensate mode, Zakharov[8] proposed the collapse of Langmuir wave packet as the mechanism to dissipate the wave energy. The Zakharov theory of Langmuir collapse[9,10] therefore presupposes that Langmuir turbulence first undergoes an inverse cascade process. However, the physics of inverse cascade of beam-generated Langmuir turbulence has been numerically studied within the context of weak turbulence theory only under the simple 1D situations.[11–14] We should note, however, that Zakharov equation itself has been solved in 2D[15] and 3D.[16] It is the set of equations of incoherent weak turbulence theory that has never been solved self-consistently in 2D.

In the solar wind, electrons up to 1 keV are routinely observed near 1 AU. These electrons are made of relatively dense and cold core (~10 eV) and an energetic component, which is in turn usually interpreted as a combination of isotropic halo and field-aligned beam.[17–25] The energetic electrons are believed to be generated during solar flares, and propagate out along the open field lines. These electrons lead to solar type III radio bursts, as already noted in the opening paragraph.[1–3] The *in situ* detection of ~1 keV energetic (halo plus beam) electrons near 1 AU is thus highly relevant to type III burst problems. It is well known that the initial beam electrons can undergo velocity-space plateau forma-

[a)]Electronic mail: ziebell@if.ufrgs.br.
[b)]Electronic mail: rudi@ufpel.edu.br.
[c)]Also at: Massachusetts Technological Laboratory, Inc., 330 Pleasant Street, Belmont, MA 02478, USA. Electronic mail: yoonp@umd.edu.

 

tion, but to account for the isotropization, it is customary to invoke pitch-angle scattering by some sort of electromagnetic fluctuation such as whistler turbulence,[26,27] or by collisional dynamics, often incorporated in the theory.[28–39]

In the present paper we report the first fully self-consistent numerical solution of weak turbulence equation in 2D. As a first step to the full generalization that includes EM modes, we first solve electrostatic (ES) *L*-*S* wave decay problem. In spite of this simplification, the present analysis includes higher-order nonlinearity that goes beyond the well-known quasilinear (QL) process. Full numerical solution of ES decay problem has never been obtained in 2D, as noted already. Even for the simple QL relaxation problem, 2D solution is rarely done in the literature. The first numerical solution of the 2D QL equation for electron beam-plasma and bump-on-tail instability problem is given in Ref. 40. In Refs. 41 and 42, 2D QL equations involving an ion beam and an ion-acoustic instability, which is similar to the bump-on-tail Langmuir instability problem from the standpoint of the numerics, was solved. There are other works pertaining to 2D numerical solutions of the QL equation,[43,44] but as far as we are aware of, the 2D decay problem that goes beyond the QL approximation has not been solved.

As it will turn out, the findings in the present discussion will be relevant to the two above-mentioned, seemingly unrelated problems of Langmuir condensation leading to strong Langmuir turbulence modulational instability and the generation of isotropic halo distribution by beam-plasma interaction. The details will be discussed next.

## II. THEORETICAL FORMULATION AND NUMERICAL SETUP

The wave kinetic equations for *L* and *S* waves that support the QL process as well as nonlinear decay processes are given in terms of the spectral wave energy density, $I_{\mathbf{k}}^{\sigma L}=\langle E_L^{\sigma 2}(\mathbf{k})\rangle$ and $I_{\mathbf{k}}^{\sigma S}=\langle E_S^{\sigma 2}(\mathbf{k})\rangle$, where $E_L^{\sigma}(\mathbf{k})$ and $E_S^{\sigma}(\mathbf{k})$ represent the spectral electric field component associated with *L* and *S* waves, respectively, and where $\sigma=\pm 1$ stands for the sign of wave phase velocity. The wave kinetic equations for these waves are given by[45]

$$\frac{\partial I_{\mathbf{k}}^{\sigma L}}{\partial t}=\frac{\pi\omega_p^2}{k^2}\int d\mathbf{v}\,\delta(\sigma\omega_{\mathbf{k}}^L-\mathbf{k}\cdot\mathbf{v})\times\left[\frac{n_0e^2}{\pi}F_e(\mathbf{v})+\sigma\omega_{\mathbf{k}}^L I_{\mathbf{k}}^{\sigma L}\mathbf{k}\cdot\frac{\partial F_e(\mathbf{v})}{\partial\mathbf{v}}\right]+\frac{\pi e^2}{2T_e^2}\sum_{\sigma',\sigma''=\pm 1}\sigma\omega_{\mathbf{k}}^L\int d\mathbf{k}'\frac{\mu_{\mathbf{k}-\mathbf{k}'}(\mathbf{k}\cdot\mathbf{k}')^2}{k^2k'^2|\mathbf{k}-\mathbf{k}'|^2}\times\delta(\sigma\omega_{\mathbf{k}}^L-\sigma'\omega_{\mathbf{k}'}^L-\sigma''\omega_{\mathbf{k}-\mathbf{k}'}^S)\left[\sigma\omega_{\mathbf{k}}^L I_{\mathbf{k}'}^{\sigma' L}\frac{I_{\mathbf{k}-\mathbf{k}'}^{\sigma'' S}}{\mu_{\mathbf{k}-\mathbf{k}'}}-\left(\sigma'\omega_{\mathbf{k}'}^L\frac{I_{\mathbf{k}-\mathbf{k}'}^{\sigma'' S}}{\mu_{\mathbf{k}-\mathbf{k}'}}+\sigma''\omega_{\mathbf{k}-\mathbf{k}'}^L I_{\mathbf{k}'}^{\sigma' L}\right)I_{\mathbf{k}}^{\sigma L}\right], \tag{1}$$

$$\frac{\partial}{\partial t}\frac{I_{\mathbf{k}}^{\sigma S}}{\mu_{\mathbf{k}}}=\frac{\pi\mu_{\mathbf{k}}\omega_p^2}{k^2}\int d\mathbf{v}\,\delta(\sigma\omega_{\mathbf{k}}^S-\mathbf{k}\cdot\mathbf{v})\left[\frac{n_0e^2}{\pi}(F_e+F_i)+\sigma\omega_{\mathbf{k}}^L\frac{I_{\mathbf{k}}^{\sigma S}}{\mu_{\mathbf{k}}}\mathbf{k}\cdot\frac{\partial}{\partial\mathbf{v}}\left(F_e+\frac{m_e}{m_i}F_i\right)\right]+\frac{\pi e^2}{4T_e^2}\sum_{\sigma',\sigma''=\pm 1}\sigma\omega_{\mathbf{k}}^L\int d\mathbf{k}'\frac{\mu_{\mathbf{k}}[\mathbf{k}'\cdot(\mathbf{k}-\mathbf{k}')]^2}{k^2k'^2|\mathbf{k}-\mathbf{k}'|^2}\times\delta(\sigma\omega_{\mathbf{k}}^S-\sigma'\omega_{\mathbf{k}'}^L-\sigma''\omega_{\mathbf{k}-\mathbf{k}'}^L)\left[\sigma\omega_{\mathbf{k}}^L I_{\mathbf{k}'}^{\sigma' L}I_{\mathbf{k}-\mathbf{k}'}^{\sigma'' L}-(\sigma'\omega_{\mathbf{k}'}^L I_{\mathbf{k}-\mathbf{k}'}^{\sigma'' L}+\sigma''\omega_{\mathbf{k}-\mathbf{k}'}^L I_{\mathbf{k}'}^{\sigma' L})\frac{I_{\mathbf{k}}^{\sigma S}}{\mu_{\mathbf{k}}}\right]. \tag{2}$$

Details about these equations can be found in Ref. 45, and references therein. Here we just explain that the first term in Eq. (1), which rules the evolution of *L* waves, describes the spontaneous emission effect and the usual quasilinear effect. The second term contains the energy conservation condition, $\delta(\sigma\omega_{\mathbf{k}}^L-\sigma'\omega_{\mathbf{k}'}^L-\sigma''\omega_{\mathbf{k}-\mathbf{k}'}^S)$, and describes the three-wave decay process. Equation (2) rules the evolution of *S* waves, and features similar terms.

The electron particle kinetic equation is given by

$$\frac{\partial F_e(\mathbf{v})}{\partial t}=\frac{\partial}{\partial v_i}\left[A_i(\mathbf{v})F_e(\mathbf{v})+D_{ij}(\mathbf{v})\frac{\partial F_e(\mathbf{v})}{\partial v_j}\right],$$

$$A_i(\mathbf{v})=\frac{e^2}{4\pi m_e}\int d\mathbf{k}\frac{k_i}{k^2}\sum_{\sigma=\pm 1}\sigma\omega_{\mathbf{k}}^L\delta(\sigma\omega_{\mathbf{k}}^L-\mathbf{k}\cdot\mathbf{v}), \tag{3}$$

$$D_{ij}(\mathbf{v})=\frac{\pi e^2}{m_e^2}\int d\mathbf{k}\frac{k_ik_j}{k^2}\sum_{\sigma=\pm 1}\delta(\sigma\omega_{\mathbf{k}}^L-\mathbf{k}\cdot\mathbf{v})I_{\mathbf{k}}^{\sigma L}.$$

The term with coefficient $A_i$ describes the effect of spontaneous fluctuations, and the term with coefficient $D_{ij}$ corresponds to the usual quasilinear effect. For the ions, it is reasonable to assume a time-stationary state. In 2D, the ion distribution is $F_i(\mathbf{v})=(2\pi T_i/m_i)^{-1/2}\exp(-m_iv^2/2T_i)$, where $T_i$ and $m_i$ stand for ion temperature and proton mass, respectively. In the above $\omega_p=(4\pi n_0e^2/m_e)^{1/2}$ is the electron plasma frequency, and $e$, $m_e$, and $n_0$ stand for the unit electric charge, electron mass, and the ambient particle number density, respectively. The dispersion relations for *L* and *S* modes are well-known, $\omega_{\mathbf{k}}^L=\omega_p(1+3k^2\lambda_D^2/2)$, and $\omega_{\mathbf{k}}^S=\omega_pk\lambda_D(m_e/m_i)^{1/2}(1+3T_i/T_e)^{1/2}(1+k^2\lambda_D^2)^{-1/2}$, where $v_e=(2T_e/m_e)^{1/2}$ is the electron thermal speed, and $\lambda_D=v_e/(\sqrt{2}\omega_p)$ is the electron Debye length, with $T_e$ being the electron temperature. In Eqs. (1) and (2) we have also introduced a quantity $\mu_{\mathbf{k}}=|k|^3\lambda_D^3(m_e/m_i)^{1/2}(1+3T_i/T_e)^{1/2}$.

We initialize the wave intensities by balancing the spontaneous and induced emissions, taking into account the background electron populations,

$$I_{\mathbf{k}}^{\sigma L}(0) = \frac{T_e}{4\pi^2}\frac{1}{1+3k^2\lambda_D^2},$$

$$I_{\mathbf{k}}^{\sigma S}(0) = \frac{T_e}{4\pi^2}k^2\lambda_D^2\sqrt{\frac{1+k^2\lambda_D^2}{1+3k^2\lambda_D^2}} \times \frac{\int d\mathbf{v}\,\delta(\sigma\omega_{\mathbf{k}}^S - \mathbf{k}\cdot\mathbf{v})(F_e+F_i)}{\int d\mathbf{v}\,\delta(\sigma\omega_{\mathbf{k}}^S - \mathbf{k}\cdot\mathbf{v})[F_e+(T_e/T_i)F_i]}. \quad (4)$$

The initial electron distribution corresponds to a combined Maxwellian background plus a tenuous component of the drifting Gaussian beam population. In 2D, it is given by $F_e(\mathbf{v},0)=(1-n_b/n_0)(\pi v_e^2)^{-1}\exp(-v^2/v_e^2)+(n_b/n_0)\times(\pi v_b^2)^{-1}\exp[-v_\perp^2/v_b^2-(v_\parallel-v_0)^2/v_b^2]$. Here $v_e^2=2T_e/m_e$ and $v_b^2=2T_b/m_e$. We have solved Eqs. (1)–(3) in 2D wave number and 2D velocity spaces, by employing the Runge–Kutta procedure with adjustable time step for the wave equations. The value of the time step obtained with the Runge–Kutta procedure is then used as the step in the particle kinetic equation, which is solved by the implicit method in an alternate direction (the so-called ADI method).

We used $51\times51$ grids for $k_\perp$ and $k_\parallel$, with $0<k_\perp v_e/\omega_p<0.5$, and $0<k_\parallel v_e/\omega_p<0.5$. For the velocities, we use $51\times51$ grids for $v_\perp/v_e$ and $51\times101$ grids for $v_\parallel/v_e$, covering the velocity range $0<v_\perp/v_e<12$ and $-12<v_\parallel/v_e<12$. For most of the following results, we assumed the ratio of beam-to-thermal electrons $n_b/n_0=2.0\times10^{-4}$, normalized beam speed $v_0/v_e=5.0$, equal beam-to-background temperature $T_b/T_e=1.0$, the electron-to-ion temperature ratio $T_e/T_i=7.0$, and the plasma parameter $(n_0\lambda_D^3)^{-1}\simeq4.47\times10^{-3}$. We deliberately chose this set of parameters, which are identical to those used in the case of our earlier 1D solution,[12] so that a direct comparison can be made between 1D and 2D cases.

## III. NUMERICAL RESULTS AND ANALYSIS

In Fig. 1 we show the evolution of electron distribution function starting from $t=0$, to $t=2\times10^3\omega_p^{-1}$, to $t=5\times10^3\omega_p^{-1}$. The well-known quasilinear plateau formation along the parallel direction can be seen to occur. However, another feature inherent to 2D nonlinear dynamics emerges, namely, Fig. 1 displays the occurrence of distinctive perpendicular broadening of the distribution function in the region of the parallel plateau. This broadening indicates that, in the presence of electrostatic fluctuations, a tendency to isotropization of the distribution takes place locally. The present finding can be considered as yet another mechanism that can be potentially applicable for isotropic solar wind electron problems. It relies on nonlinear mechanisms, while other isotropization mechanisms, like the whistler pitch-angle theory discussed in Refs. 26 and 27, are essentially quasilinear.

Figures 2 and 3 display the spectra of $L$ and $S$ waves for $\omega_p t=500$, 2000, and 5000. We chose to show the starting $L$ and $S$ wave spectra at $\omega_p t=500$ rather than at $t=0$ because initially the wave intensities are rather low, and do not show any interesting features.

Figure 2 shows the appearance of a peak in the Langmuir spectrum which is already quite prominent at

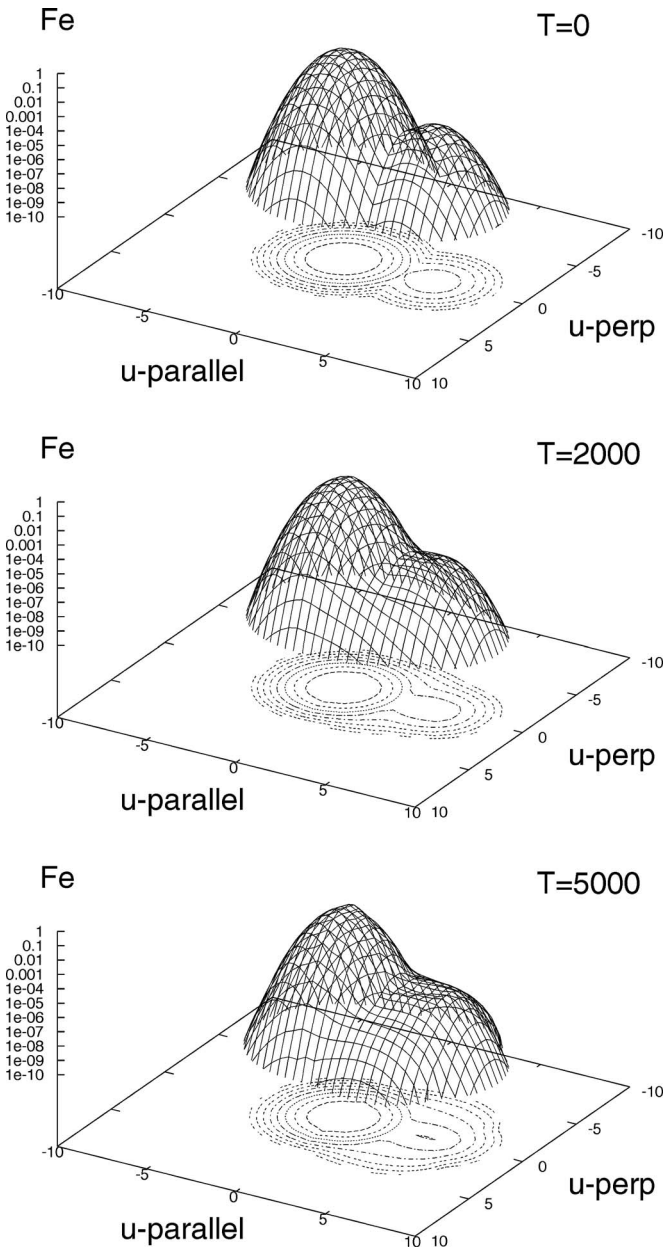


FIG. 1. Electron distribution function, $F_e(v_\perp,v_\parallel,0)$, vs $v_\perp/v_e$ and $v_\parallel/v_e$, in the vertical logarithmic scale; (top) initial electron distribution; (middle) the electron distribution at $\omega_p t=2\times10^3$; and (bottom) at $\omega_p t=5\times10^3$.

$\omega_p t=500$. This time period is relatively early in the nonlinear stage, and can be viewed as dominated by the quasilinear process. The peak, which constitutes the so-called primary Langmuir spectrum, is centered at $k_\perp=0$ and $k_\parallel v_e/\omega_p\simeq0.2$, in accordance with linear growth theory. Note that the 2D spectrum features much broader spread along $k_\perp$ than along $k_\parallel$. If we were to project the results to 1D $k_\parallel$ axis, then the primary Langmuir turbulence spectrum would be qualitatively similar to that obtained with the 1D approximation. In addition to the primary spectrum, Fig. 2 also shows a slight enhancement in the backward propagating direction with peak spectrum occurring at $k_\parallel v_e/\omega_p\simeq-0.2$. This enhancement is barely visible at the first panel of Fig. 1, but is already perfectly noticeable in the second panel, which shows the wave spectrum at $\omega_p t=2\times10^3$. The asymmetric

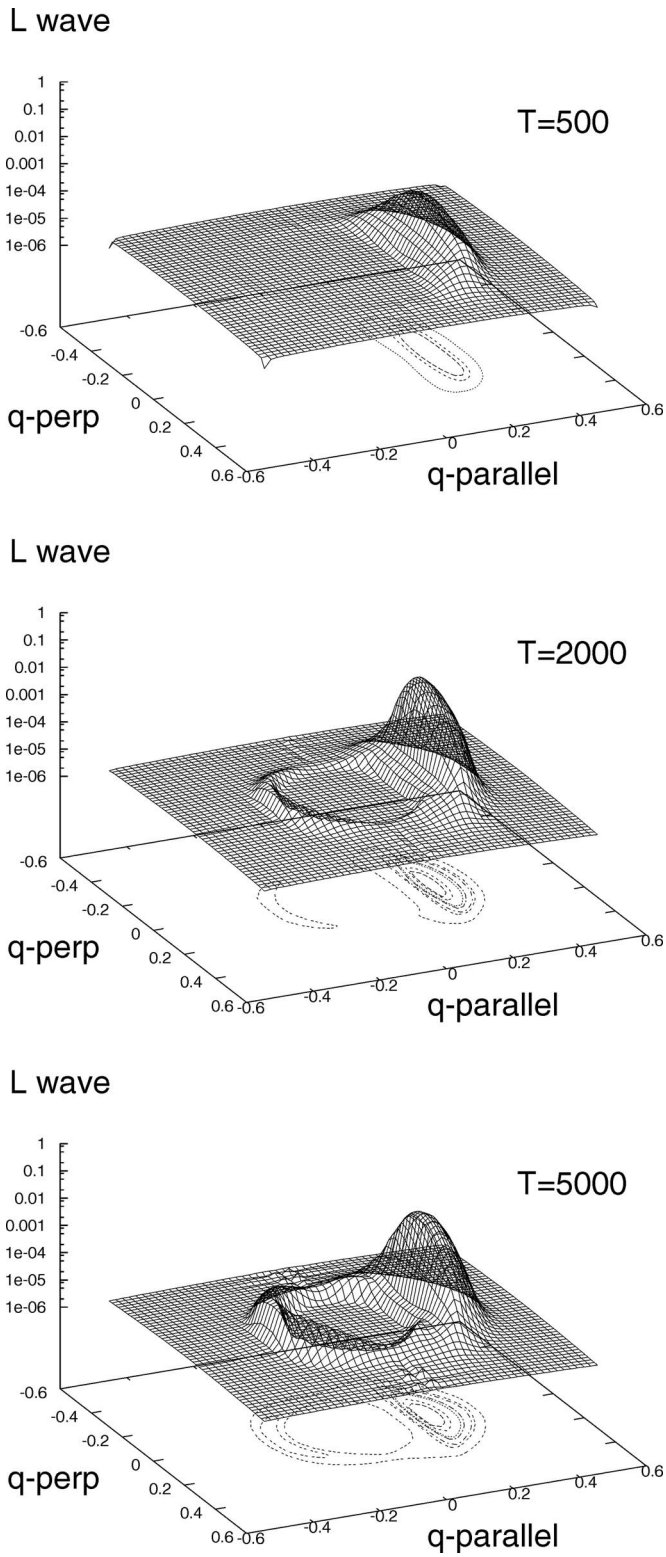


FIG. 2. $L$ wave intensity, at $\omega_p t=500$ (top), $\omega_p t=2\times10^3$ (middle), and at $\omega_p t=5\times10^3$, vs $k_\perp v_e/\omega_p$ and $k_\parallel v_e/\omega_p$, in the vertical logarithmic scale.

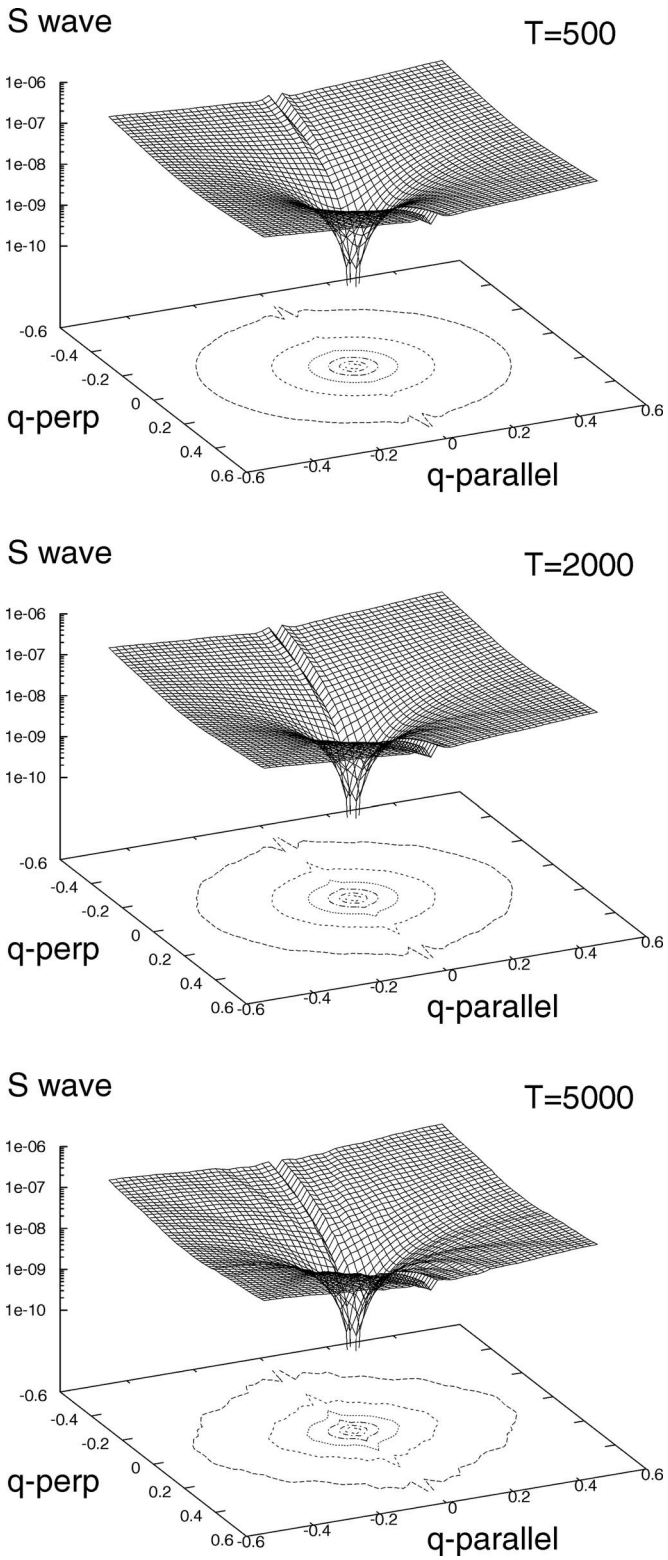


FIG. 3. $S$ wave intensity, at $\omega_p t=500$ (top), $\omega_p t=2\times10^3$ (middle), and at $\omega_p t=5\times10^3$, vs $k_\perp v_e/\omega_p$ and $k_\parallel v_e/\omega_p$, in the vertical logarithmic scale.

twin-peaked structure is again reminiscent of the 1D analysis.[12] However, the backward peak is also quite broadened in the perpendicular direction. Considering both the forward and the backward peaks, the notable feature which emerges in the 2D analysis is that the two peaks constitute a large area in wave number space along a circumference, where the waves are able to grow. This is an indication that nonlinear decay process is already at work.

The middle and lower panels in Fig. 2 show later stages of Langmuir wave decay dynamics (at $\omega_p t=2\times10^3$ and at $\omega_p t=5\times10^3$, respectively). While the primary Langmuir waves are still seen to grow at $\omega_p t=2000$, by the time that

the system has evolved to $\omega_p t=5000$, Fig. 2 shows that the forward-propagating primary Langmuir waves have practically ceased to grow, indicating saturation. The backward peak, on the other hand, continues to evolve between $\omega_p t=2000$ and $\omega_p t=5000$. The circular ringlike structure in the spectrum of Langmuir waves also continues to grow between $\omega_p t=2000$ and $\omega_p t=5000$, as a result of 2D decay, and becomes more prominent. At the later stage of our computation, the ring spectrum is a fully formed structure. Of course, this feature could not have been predicted by simple 1D analysis.

Of particular significance is that the three-wave decay process in the present 2D situation apparently does not lead to the growth of long wavelength Langmuir waves, which was observed in our earlier 1D analysis.[12] This does not mean that the decay process is ineffective in 2D when compared with the 1D situation. The point is that the decay of primary Langmuir waves, $L$, may be said to involve two processes. One of these processes is related to the generation of backscattered Langmuir waves, $L'$, that have similar wavelength but propagates in the antibeam direction, while the other would involve the generation of small $k$, long-wavelength, Langmuir condensate mode. The backscattering process, $L \rightarrow L'+S$ is evidently quite effective, as Fig. 2 indicates. As a matter of fact, the backscattering process seems to be even more robust in the present 2D case than in the 1D case. In 1D situation, the $L'$ mode generation is limited strictly to the antiparallel mode, while, as Fig. 2 demonstrates, in the present 2D case the $L'$ mode can now spread around the circular ring area in 2D wave number space. In contrast, the generation of long wavelength waves (i.e., the inverse cascade process) appears as less effective in the present 2D case than in the 1D case.

We observe from Fig. 3 that the $S$ wave turbulence spectrum develops some ripples along the time evolution but does not actually grow above the initial fluctuation level. Thus, the $S$ mode turbulence features nothing special as far as the spectrum is concerned, for the parameters considered. However, it is important to note that even though the $S$ waves do not get amplified, they nevertheless participate in the nonlinear three-wave dynamics. It is also possible to infer that the absence of growth of the $S$ waves should not to be regarded as indication of low efficiency of the decay process, since similar low level of excitation of $S$ waves has also been obtained in the case of 1D analysis.[12]

These results obtained from 2D dynamics can be projected into 1D space, by integration over the perpendicular variables. We define the 1D electron distribution function and wave intensities, as follows:

$$F_{e,1\mathrm{D}}(v_\parallel,t)=\int dv_\perp F_e(v_\parallel,v_\perp,t),$$

$$I^{\sigma\alpha}_{\mathbf{k},1\mathrm{D}}(k_\parallel,t)=\int dk_\perp I^{\sigma\alpha}_{\mathbf{k}}(k_\parallel,k_\perp,t). \tag{5}$$

Figure 4(a) shows $F_{e,1\mathrm{D}}$ vs $v_\parallel/v_e$, for $\omega_p t=0$, 500, $1\times10^3$, $3\times10^3$, and $5\times10^3$. The formation of a plateau in the beam region of the distribution is clearly noticeable. Figure 4(b) shows $I^{\sigma L}_{\mathbf{k},1\mathrm{D}}$ vs $q_\parallel=k_\parallel v_e/\omega_p$, for the same moments in time which appeared in panel (a), namely $\omega_p t=0$, 500, $1\times10^3$, $3\times10^3$, and $5\times10^3$. It is seen that the fast growth of the peak at $k_\parallel v_e/\omega_p\simeq0.2$, which is already noticeable at $\omega_p t=500$, and the appearance of a much smaller peak corresponding to backward propagating waves, at $k_\parallel v_e/\omega_p\simeq-0.2$.

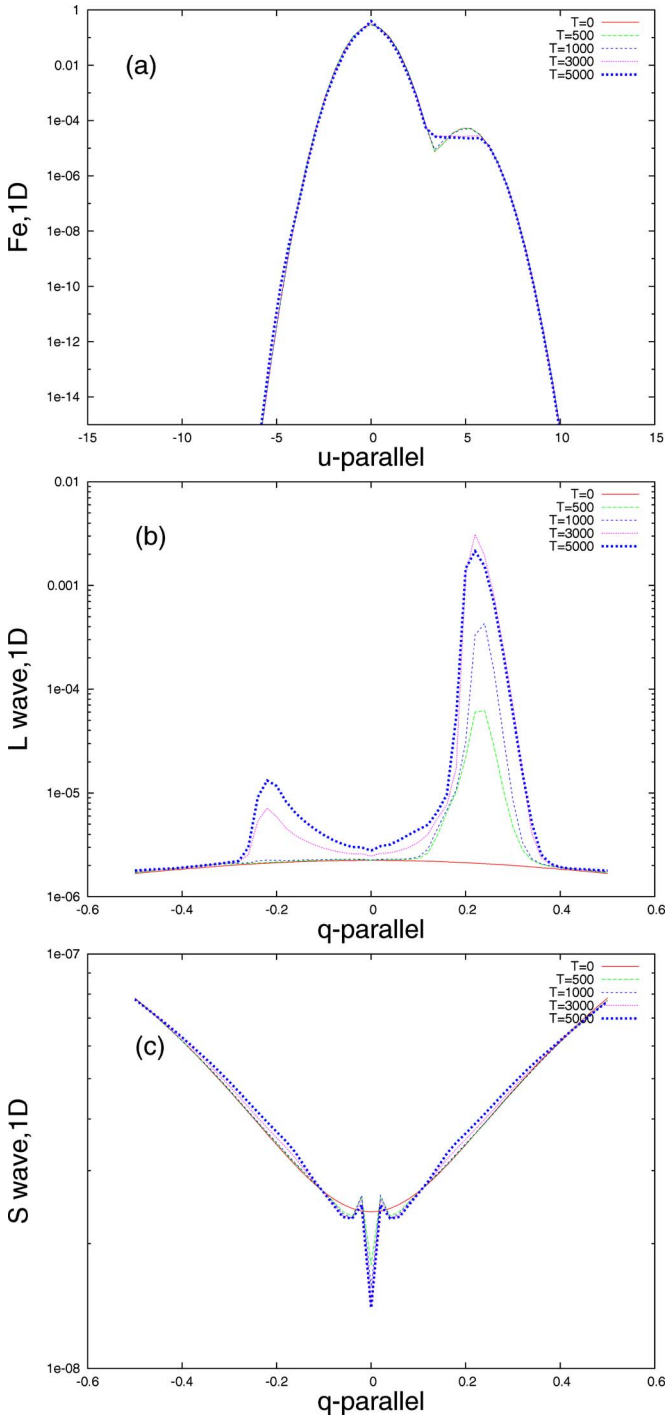


FIG. 4. (Color online) 1D electron distribution function and $L$ and $S$ wave intensities, obtained considering quasilinear and three-wave decay processes. (a) $F_{e,1\mathrm{D}}$ at $\omega_p t=0$, $5\times10^2$, $1\times10^3$, $2\times10^3$, $3\times10^3$, and $5\times10^3$, vs $v_\parallel/v_e$, in the vertical logarithmic scale. (b) $L$ wave intensity, at $\omega_p t=0$, $5\times10^2$, $1\times10^3$, $3\times10^3$, and $5\times10^3$, vs $k_\parallel v_e/\omega_p$, in the vertical logarithmic scale. (c) $S$ wave intensity, at $\omega_p t=0$, $5\times10^2$, $1\times10^3$, $3\times10^3$, and $5\times10^3$, vs $k_\parallel v_e/\omega_p$, in the vertical logarithmic scale.

The backward peak starts very inconspicuous, and only becomes really noticeable at $\omega_p t \simeq 3000$. These two peaks continue to grow, at different rates, so that the asymmetry between forward and backward peaks is considerably reduced at the late stages of our calculation, at $\omega_p t = 5 \times 10^3$. It is also seen the appearance of sizable values of $I^{\sigma L}_{\mathbf{k},1\mathrm{D}}$ for small values of $k_\parallel$, at the late stages of the calculation. As mentioned before, this 1D projection of the results may lead to the interpretation of inverse cascading process, but the 2D results appearing in Fig. 2 show that this is only an effect of the projection to 1D. In other words, these results show that the 1D projection along $k_\parallel$ of the circular ringlike structure obtained in 2D wave number space may lead to the interpretation of Langmuir waves inverse cascading into the long-wavelength regime. However, the 2D results show the actual wavelength does not increase at all, but only the wave propagation direction changes.

Figure 4(c) shows $I^{\sigma S}_{\mathbf{k},1\mathrm{D}}$ vs $q_\parallel = k_\parallel v_e / \omega_p$, for $\omega_p t = 0$, 500, $1 \times 10^3$, $3 \times 10^3$, and $5 \times 10^3$. It is seen that the spectrum of ion-sound waves remains nearly featureless along the time evolution, as already seen in the 2D depiction appearing in Fig. 3.

For comparison, we have also obtained results considering only the quasilinear dynamics, that is, by neglecting the terms corresponding to three-wave decay in Eqs. (1) and (2). Figure 5 shows the results obtained, for the same times and parameters used for Fig. 4. Figure 5(a) shows a formation of a plateau in the electron distribution function similar to that depicted in Fig. 4(a). This indicates that, for the parameters and situation considered, the dynamics of the electron distribution function is mostly ruled by the quasilinear process. This should be expected, since higher order effects were neglected in the equation for the evolution of the electron distribution function, Eq. (3).

The corresponding spectra of $L$ waves are seen in Fig. 5(b), which shows the growth of the amplitude of forward-propagating $L$ waves, without the appearance of backward waves or significant amplitude in the region of small $k_\parallel$. These two features appear in Fig. 4(b), which indicates that they occur due to decay processes. The evolution of the ion-sound wave spectrum is displayed in Fig. 5(c), which appears virtually the same as Fig. 4(c).

The effect of the $S$ waves on the three-wave decay process can be further investigated. As already mentioned, the results appearing in Fig. 3 show that the spectrum of $S$ waves does not grow appreciably above the initial level. However, the ion-sound waves play a very important role on the decay process of $L$ waves. This point can be illustrated by the consideration of a rather artificial case in which we assume that the equilibrium level of $S$ waves is higher than the level predicted by the balance condition given by Eq. (5). For instance, let us assume a case in which the equilibrium level of $S$ waves is higher by a factor 100 as compared to the case considered in Figs. 1–5, with all the other parameters remaining the same.

Figure 6 shows the ensuing evolution of electron distribution function starting from $t=0$, to $t = 2 \times 10^3 \omega_p^{-1}$, to $t = 5 \times 10^3 \omega_p^{-1}$. As in the case appearing in Fig. 1, the quasilinear plateau formation along parallel direction is seen to occur.

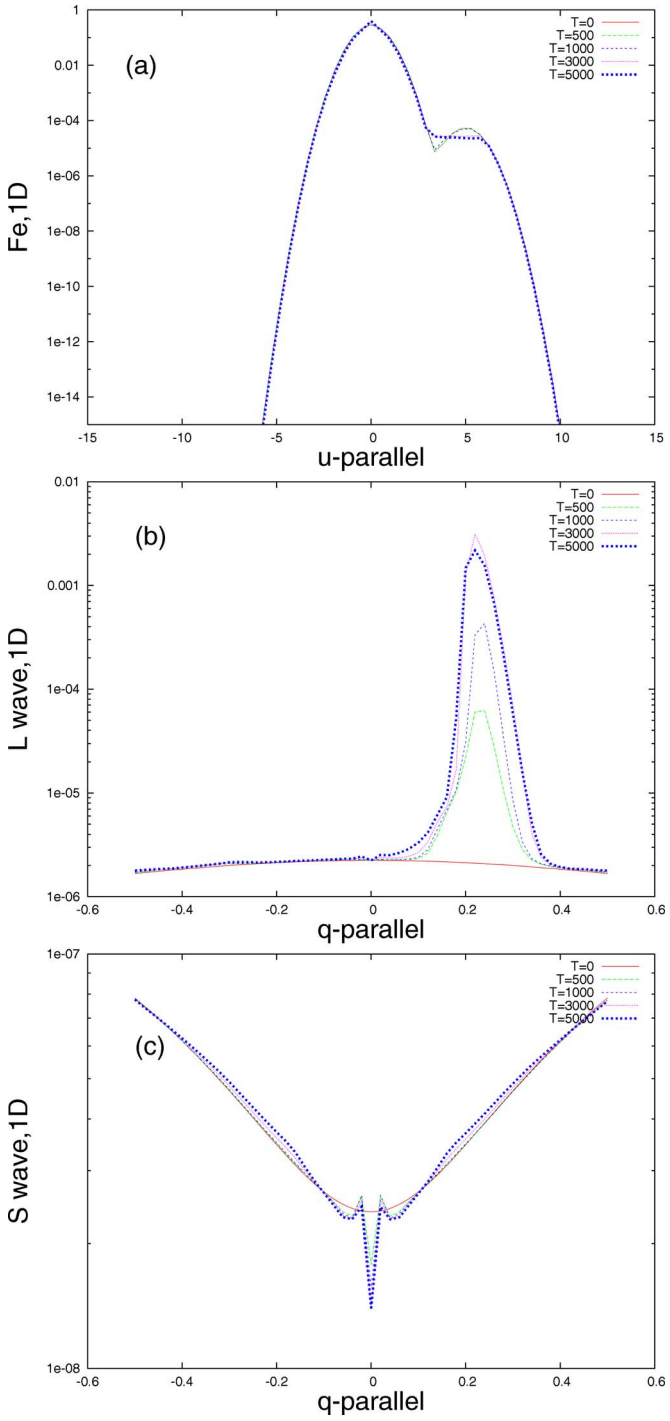


FIG. 5. (Color online) 1D electron distribution function and $L$ and $S$ wave intensities, obtained considering only quasilinear processes. (a) $F_{e,1\mathrm{D}}$ at $\omega_p t = 0$, $5 \times 10^2$, $1 \times 10^3$, $2 \times 10^3$, $3 \times 10^3$, and $5 \times 10^3$, vs $v_\parallel / v_e$, in the vertical logarithmic scale. (b) $L$ wave intensity, at, $5 \times 10^2$, $1 \times 10^3$, $3 \times 10^3$, and $5 \times 10^3$, vs $k_\parallel v_e / \omega_p$, in vertical logarithmic scale. (c) $S$ wave intensity, at $\omega_p t = 0$, $5 \times 10^2$, $1 \times 10^3$, $3 \times 10^3$, and $5 \times 10^3$, vs $k_\parallel v_e / \omega_p$, in the vertical logarithmic scale.

Other distinctive feature appearing in Fig. 1 and in Fig. 6 is the perpendicular broadening of the distribution function in the region of the parallel plateau, indicating a tendency to isotropization of the distribution function taking place in the presence of electrostatic fluctuations. However, Fig. 6 shows that the corresponding effect is much larger in the case of

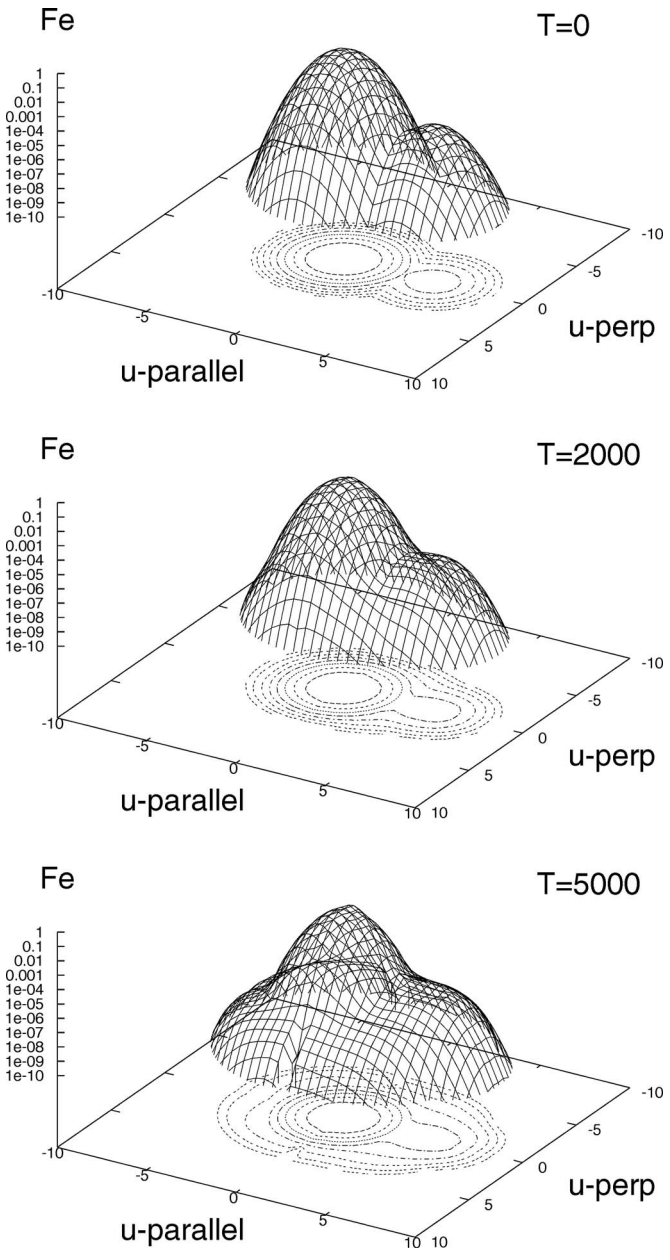


FIG. 6. Electron distribution function, $F_e(v_\perp, v_\parallel, 0)$, vs $v_\perp/v_e$ and $v_\parallel/v_e$, in the vertical logarithmic scale; (top) initial electron distribution; (middle) the electron distribution at $\omega_p t = 2\times 10^3$; and (bottom) at $\omega_p t = 5\times 10^3$. The equilibrium level of $S$ waves is 100 times the level assumed in the case of Fig. 1. Other parameters are the same as in Fig. 1.

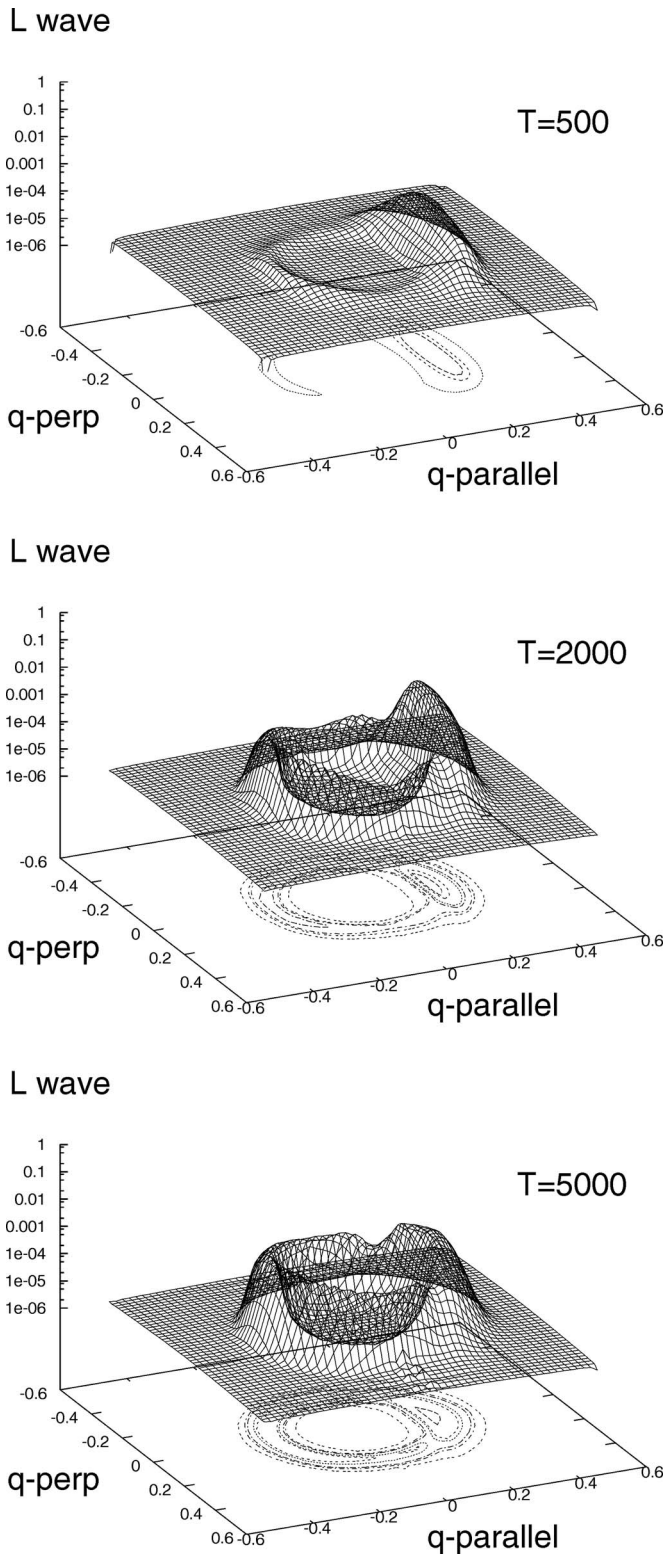


FIG. 7. $L$ wave intensity, at $\omega_p t = 500$ (top), $\omega_p t = 2\times 10^3$ (middle), and at $\omega_p t = 5\times 10^3$, vs $k_\perp v_e/\omega_p$ and $k_\parallel v_e/\omega_p$, in the vertical logarithmic scale. The parameters are the same as in Fig. 6.

enhanced $S$ waves. Figure 6 even displays the appearance of a backward tail as well as heating along $v_\perp$. The backward tail and the perpendicular heating together form a quasi-isotropic shoulder in the distribution function. This shoulder is intimately related to the 2D dynamics of the electrostatic decay processes, which cannot be discussed with 1D theory, locally.

Figure 7 displays the spectrum of $L$ waves, shown at the same moments of the time evolution as those depicted in Fig. 2. The first panel of Fig. 7 shows the appearance of the primary peak of the Langmuir spectrum, quite prominent at $\omega_p t = 500$, and similar to that appearing in the first panel of Fig. 2. The first panel of Fig. 7 also shows a smaller peak in the backward propagating direction. Although smaller than the primary peak, this secondary peak is more prominent than the corresponding peak appearing in Fig. 2. Since the secondary peak is formed due to nonlinear processes, this finding clearly indicates the enhancement of the efficiency of

the nonlinear process (in the present case, the three-wave decay) due to the increased level of ion-sound waves considered for Fig. 7. The middle and lower panels in Fig. 7 show the cases of $\omega_p t=2\times10^3$ and at $\omega_p t=5\times10^3$, respectively. As in the case of Fig. 2, the primary Langmuir waves are still seen to grow at $\omega_p t=2000$ and saturate at $\omega_p t=5000$. The backward peak continues to evolve between $\omega_p t=2000$ and $\omega_p t=5000$. The circular ringlike structure in the spectrum of Langmuir waves also continues to grow between $\omega_p t=2000$ and $\omega_p t=5000$, as a result of 2D decay. The whole nonlinear evolution is similar to that occurring in the case of lower level of $S$ waves, but the increased level of $S$ waves enhanced the efficiency of the process. As a consequence, at the late stage of the computation of this case of high level of ion-sound turbulence, the ring spectrum of $L$ waves is fully formed and almost isotropic, only featuring as prominent the still higher level of the primary peak. It is also noticeable that the three-wave decay process in the present 2D situation with high level of $S$ waves also does not lead to the growth of long wavelength Langmuir waves, similarly to the observation made in the case of low level of $S$ waves.

The evolution of the $S$ wave spectrum in the case of higher equilibrium level of $S$ waves is qualitatively similar to that obtained in the case of low equilibrium level. Figure 8 shows that the $S$ wave turbulence spectrum develops some ripples along the time evolution but does not actually grow above the initial fluctuation level. The same observation is made related to Fig. 3, relative to the low level case.

Another aspect related to the effect of $S$ waves on the three-wave decay process is illustrated by Fig. 9, which has been obtained considering the ratio electron-to-ion temperature $T_e/T_i=20$, and other parameters equal to those used to obtain Figs. 1–5. The first panel of Fig. 9 depicts the electron distribution function at $\omega_p t=5\times10^3$. It is very similar to the result shown in the third panel of Fig. 1, but it shows an enhanced effect of perpendicular heating in the distribution function. The bottom panel of Fig. 9 shows the $S$ wave spectrum at $\omega_p t=5\times10^3$, and shall be compared with the third panel of Fig. 3. It is noticed that the two results are similar, but for higher value of $T_e/T_i$ the $S$ wave spectrum features enhanced level of ripples and fluctuations. Such result should be expected, since for higher electron-to-ion temperature ratio the $S$ waves are less efficiently damped by the electron population. With enhanced level of activity in the $S$ wave spectrum, the three-wave decay process becomes more efficient, and the consequence appears in the middle panel of Fig. 9, which shows the $L$ wave spectrum at $\omega_p t=5\times10^3$, to be compared to the third panel of Fig. 2. It is noticed that the formation of the ringlike structure in the $L$ spectrum is more noticeable in Fig. 9 than in Fig. 2, indicating more efficiency of the decay process.

Figure 10 illustrates the effect of higher level of spontaneous fluctuations. It has been obtained considering the plasma parameter $(n_0\lambda_D^3)^{-1}\simeq1.0\times10^{-2}$, and other parameters equal to those used to obtain Figs. 1–5. The first panel of Fig. 10 depicts the electron distribution function at $\omega_p t=5\times10^3$. It is very similar to the result shown in the third panel of Fig. 1, but it is possible to notice an enhanced effect of perpendicular heating in the distribution function. The second panel of Fig. 10 shows the $L$ wave spectrum at $\omega_p t=5\times10^3$, and shall be compared with the third panel of Fig. 2, obtained with a smaller level of spontaneous fluctuations. It is noticed that for a higher value of the plasma parameter the primary quasilinear peak does not grow so

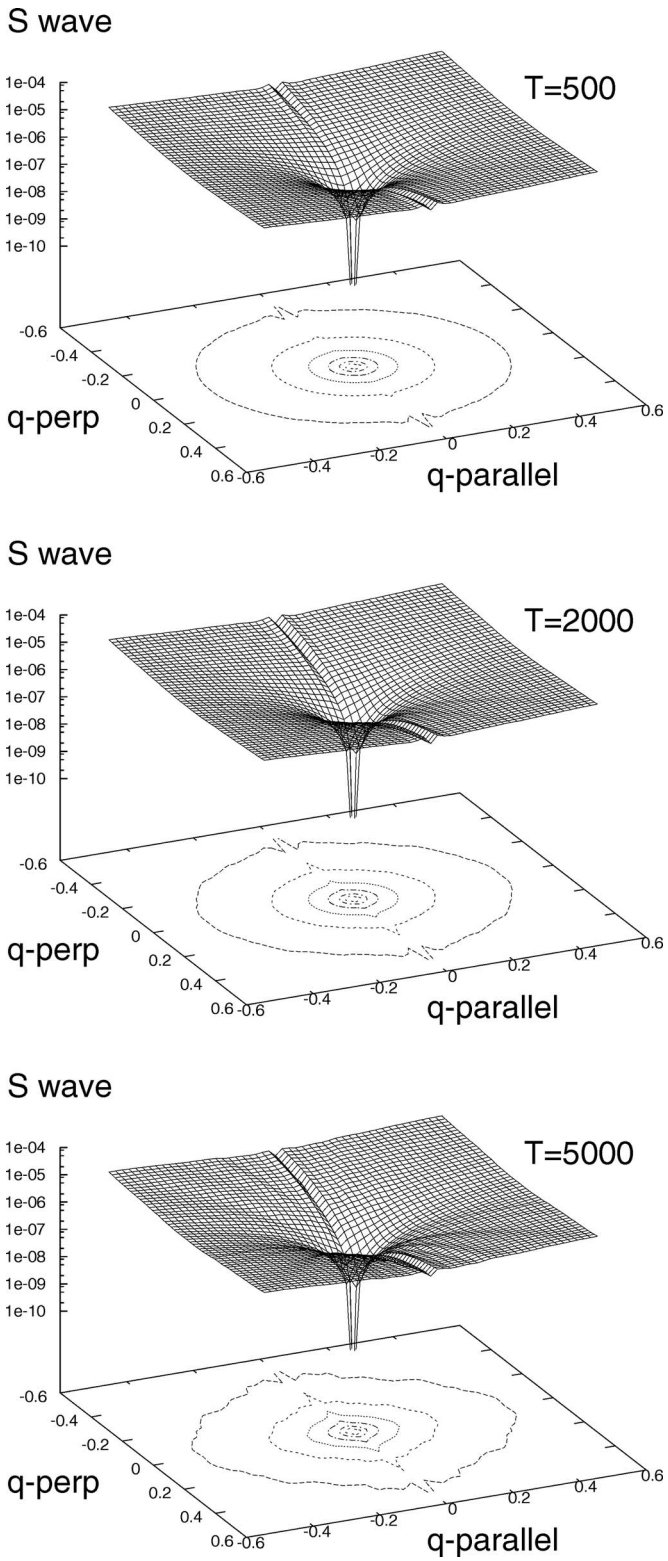


FIG. 8. $S$ wave intensity, at $\omega_p t=500$ (top), $\omega_p t=2\times10^3$ (middle), and at $\omega_p t=5\times10^3$, vs $k_\perp v_e/\omega_p$ and $k_\parallel v_e/\omega_p$, in the vertical logarithmic scale. The parameters are the same as in Fig. 6.

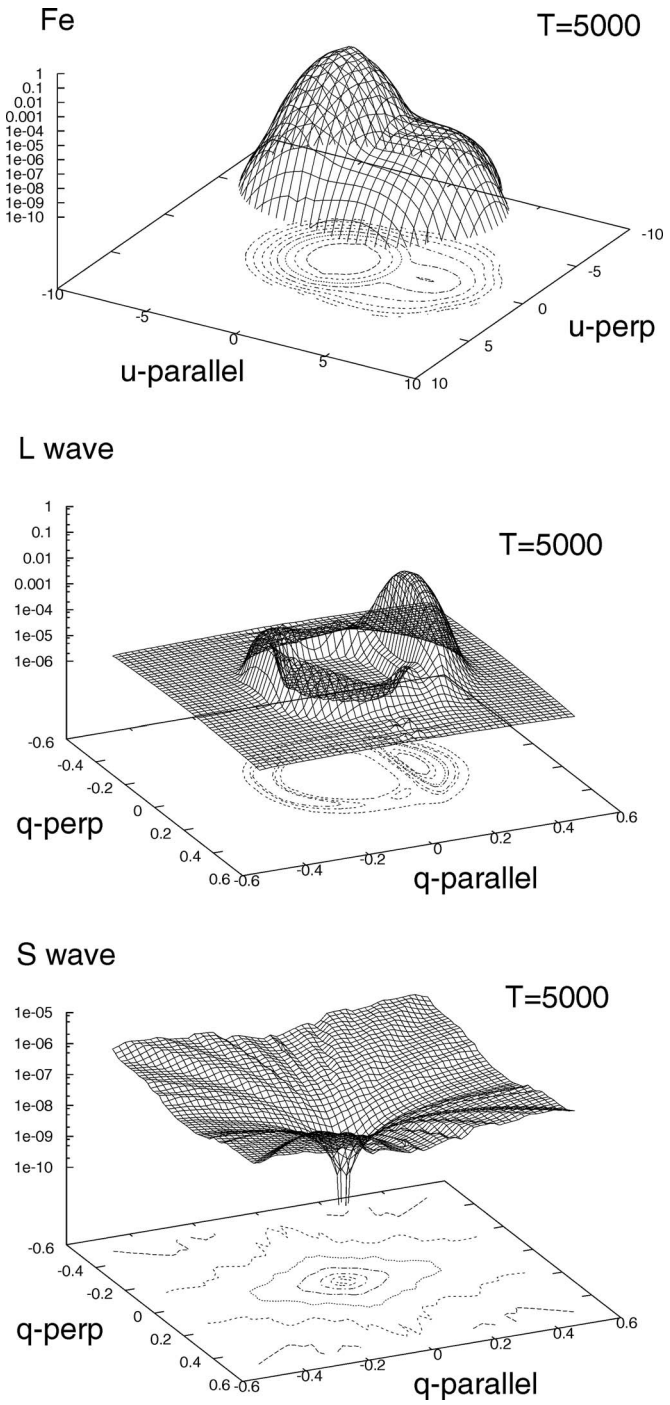


FIG. 9. (Top) Electron distribution function, $F_e(v_\perp, v_\parallel, 0)$, at $\omega_p t = 5 \times 10^3$, vs $v_\perp / v_e$ and $v_\parallel / v_e$, in the vertical logarithmic scale; (middle) $L$ wave intensity, at $\omega_p t = 5 \times 10^3$, vs $k_\perp v_e / \omega_p$ and $k_\parallel v_e / \omega_p$, in the vertical logarithmic scale; (bottom) $S$ wave intensity, at $\omega_p t = 5 \times 10^3$, vs $k_\perp v_e / \omega_p$ and $k_\parallel v_e / \omega_p$, in the vertical logarithmic scale; The ratio of electron and ion temperatures is $T_e / T_i = 20$, and other parameters are the same as in Fig. 1.

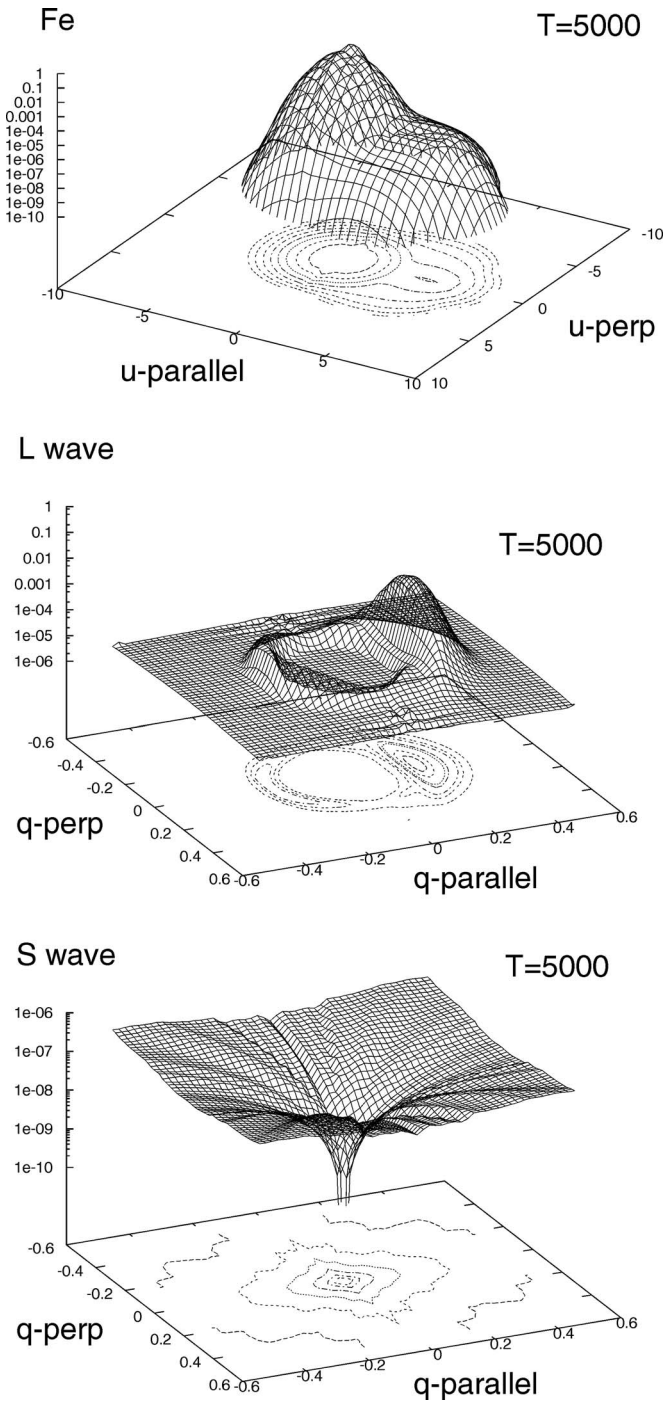


FIG. 10. (Top) Electron distribution function, $F_e(v_\perp, v_\parallel, 0)$, at $\omega_p t = 5 \times 10^3$, vs $v_\perp / v_e$ and $v_\parallel / v_e$, in the vertical logarithmic scale; (middle) $L$ wave intensity, at $\omega_p t = 5 \times 10^3$, vs $k_\perp v_e / \omega_p$ and $k_\parallel v_e / \omega_p$, in the vertical logarithmic scale; (bottom) $S$ wave intensity, at $\omega_p t = 5 \times 10^3$, vs $k_\perp v_e / \omega_p$ and $k_\parallel v_e / \omega_p$, in the vertical logarithmic scale. The plasma parameter is $(n_0 \lambda_D^3)^{-1} \simeq 1.0 \times 10^{-2}$, and other parameters are the same as in Fig. 1.

much above the already higher equilibrium level, with the result that the formation of the ringlike structure in the $L$ spectrum is more noticeable in Fig. 10 than in Fig. 2. The third panel of Fig. 10 shows the $S$ wave spectrum at $\omega_p t = 5 \times 10^3$, and shall be compared with the third panel of Fig. 3. It is noticed that the two results are similar, but for higher value of the plasma parameter the $S$ wave spectrum features slightly enhanced level of ripples and fluctuations.

Finally, Fig. 11 illustrates the effect of higher value of the ratio beam-to-thermal electrons. It has been obtained considering the ratio $n_b / n_0 = 5.0 \times 10^{-4}$, and other parameters equal to those used to obtain Figs. 1–5. The comparison between the second panel of Fig. 11 and the third panel of Fig. 2 shows that the increase in the beam population increases the effectiveness of the process of formation of the ringlike structure in the spectrum of $L$ waves. Regarding the $S$ waves,

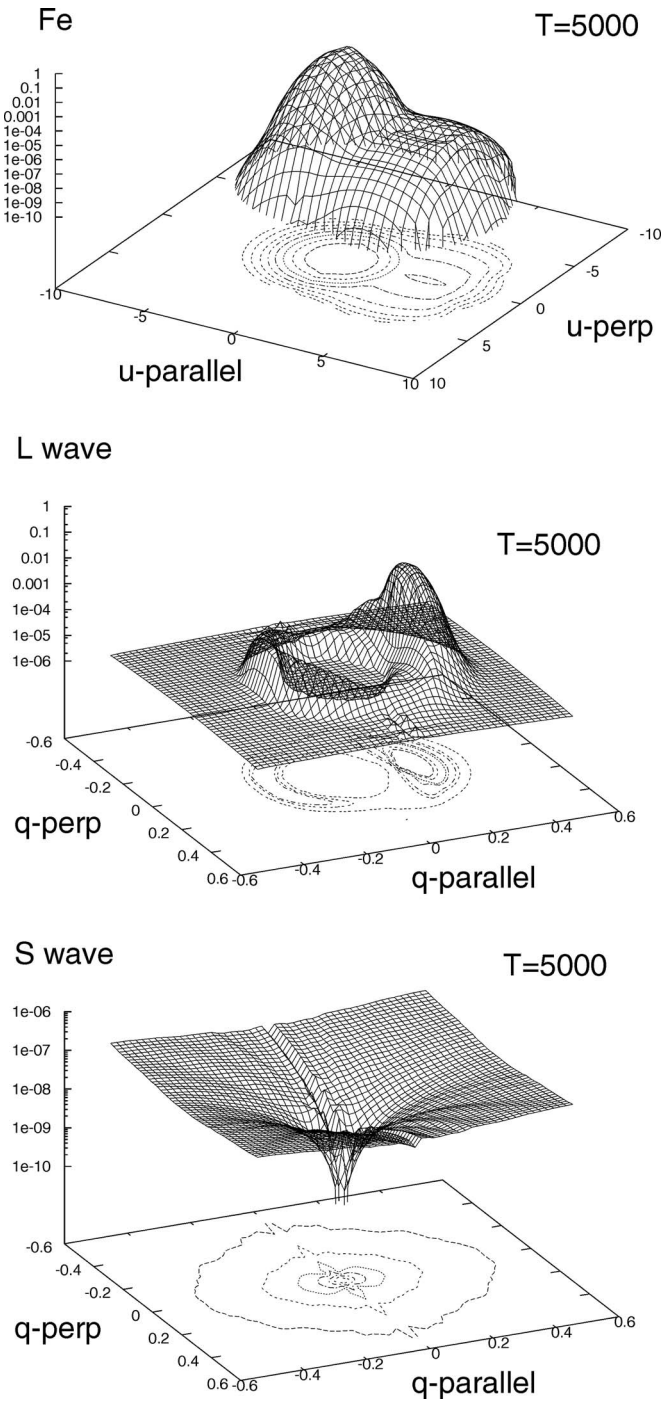


FIG. 11. (Top) Electron distribution function, $F_e(v_\perp, v_\parallel, 0)$, at $\omega_p t = 5 \times 10^3$, vs $v_\perp / v_e$ and $v_\parallel / v_e$, in the vertical logarithmic scale; (middle) $L$ wave intensity, at $\omega_p t = 5 \times 10^3$, vs $k_\perp v_e / \omega_p$ and $k_\parallel v_e / \omega_p$, in the vertical logarithmic scale; (bottom) $S$ wave intensity, at $\omega_p t = 5 \times 10^3$, vs $k_\perp v_e / \omega_p$ and $k_\parallel v_e / \omega_p$, in the vertical logarithmic scale; The ratio of beam-to-thermal electrons is $n_b / n_0 = 5.0 \times 10^{-4}$, and other parameters are the same as in Fig. 1.

it is seen that the spectra of the third panel of Fig. 11 and of the third panel of Fig. 3 are basically the same, indicating that the increased population of beam electrons did not affect the evolution of $S$ waves. On the other hand, the electron distribution function appearing in the top panel of Fig. 11 shows increased effect of perpendicular heating, as compared to the distribution in the third panel of Fig. 1, obtained with a smaller population of beam electrons.

## IV. CONCLUSION

In the present paper, we have presented results for the fully self-consistent weak turbulence equation, including nonlinear mode-coupling terms, obtained for the first time from a 2D analysis. More specifically, the results discussed in the present paper have been obtained considering quasilinear and three-wave decay processes.

Among the results obtained is the demonstration that the Langmuir turbulence in 2D situation leads to the formation of a ringlike structure in the spectra of Langmuir waves, centered at wave-number $\mathbf{k}$ such that $k v_e / \omega_p \simeq v_e / v_0$, where $v_e$ is the electron thermal speed and $v_0$ is the beam speed, and apparently does not lead to condensation effects (at least under the present parameters, and for the present approximation of excluding scattering terms in the wave equation), although these appear to occur when the results obtained in 2D are projected along the direction parallel to the beam velocity. The formation of the ringlike feature in the $L$ wave spectrum is accompanied by perpendicular heating of the electron distribution function, particularly at the region of formation of the parallel plateau in the region of the electron beam. Both features, the ringlike structure in the spectrum of $L$ waves and the perpendicular heating of the distribution, are enhanced for higher levels of the equilibrium ion-sound spectrum. The formation of the ringlike structure has also been shown to be favored by the increase of the level of spontaneous fluctuations and by the electron-to-ion temperature ratio, which are related to the level of ion-sound waves, and by the increase in the beam electron population. The results obtained also have demonstrated that for the range of parameters considered the spectrum of ion-sound waves do not grow significantly above the assumed equilibrium level, but is of paramount importance to the effectiveness of the three-wave decay process.

These results call for further exploration of the nonlinear effects in two dimensions. To proceed with the exploration of 2D effects on Langmuir turbulence, it is necessary to include the other important nonlinear process that is known to lead to long-wavelength Langmuir condensation, namely, the spontaneous and induced scattering of thermal ions. It may also be useful to compare the present findings with full 2D particle simulations. In this regard, the 2D simulation by Dum[46] is noteworthy. However, the physical parameters are quite different from those utilized in the present work, so that the results obtained cannot be easily compared. This situation therefore calls for more detailed simulations in the future. These tasks obviously belong to our future work.

## ACKNOWLEDGMENTS

This work has been partially supported by the Brazilian agencies Conselho Nacional de Desenvolvimento Científico e Tecnológico (CNPq) and Fundação para o Amparo da Pesquisa no Estado do Rio Grande do Sul (FAPERGS). P.H.Y. acknowledges support by AFOSR grant FA9550-07-0053.

[1]M. V. Goldman, Sol. Phys. **89**, 403 (1983).
[2]D. B. Melrose, in *Solar Radiophysics*, edited by D. J. McLean and N. R. Labrum (Cambridge University Press, New York, 1985), p. 37.
[3]P. A. Robinson and I. H. Cairns, Sol. Phys. **181**, 363 (1998); **181**, 395 (1998); **181**, 429 (1998).
[4]A. J. Willes, P. A. Robinson, and D. B. Melrose, Phys. Plasmas **3**, 149 (1996).
[5]B. Li, A. J. Willes, P. A. Robinson, and I. H. Cairns, Phys. Plasmas **12**, 012103 (2005).
[6]B. Li, A. J. Willes, P. A. Robinson, and I. H. Cairns, Phys. Plasmas **12**, 052324 (2005).
[7]B. Li, P. A. Robinson, and I. H. Cairns, Phys. Plasmas **13**, 092902 (2006).
[8]V. E. Zakharov, Sov. Phys. JETP **35**, 908 (1972).
[9]M. V. Goldman, Rev. Mod. Phys. **56**, 709 (1984).
[10]P. A. Robinson, Rev. Mod. Phys. **69**, 507 (1997).
[11]L. Muschietti and C. T. Dum, Phys. Fluids B **3**, 1968 (1991).
[12]L. F. Ziebell, R. Gaelzer, and P. H. Yoon, Phys. Plasmas **8**, 3982 (2001).
[13]E. P. Kontar and H. L. Pécseli, Phys. Rev. E **65**, 066408 (2002).
[14]B. Li, A. J. Willes, P. A. Robinson, and I. H. Cairns, Phys. Plasmas **10**, 2748 (2003).
[15]D. A. Russel, D. F. DuBois, and H. A. Rose, Phys. Rev. Lett. **60**, 581 (1988).
[16]D. L. Newman, P. A. Robinson, and M. V. Goldman, Phys. Rev. Lett. **62**, 2132 (1989).
[17]M. D. Montgomery, S. J. Bame, and A. J. Hundhausen, J. Geophys. Res. **73**, 4999, DOI: 10.1029/JA073i015p04999 (1968).
[18]W. C. Feldman, J. R. Asbridge, S. J. Bame, M. D. Montgomery, and S. P. Gary, J. Geophys. Res. **80**, 4181, DOI: 10.1029/JA080i031p04181 (1975).
[19]R. P. Lin, D. W. Potter, D. A. Gurnett, and F. L. Scarf, Astrophys. J. **251**, 364 (1981).
[20]R. P. Lin, W. K. Levedahl, W. Lotko, D. A. Gurnett, and F. L. Scarf, Astrophys. J. **308**, 954 (1986).
[21]W. G. Pilipp, H. Miggennieder, M. S. Montgomery, K.-H. Mühläuser, H. Rosenbauer, and R. Schwenn, J. Geophys. Res. **92**, 1075, DOI: 10.1029/JA092iA02p01075 (1987).
[22]R. J. Fitzenreiter, J. D. Scudder, and A. J. Klimas, J. Geophys. Res. **95**, 4155, DOI: 10.1029/JA095iA04p04155 (1990).
[23]R. J. Fitzenreiter, K. W. Ogilvie, D. J. Chornay, and J. Keller, Geophys. Res. Lett. **25**, 249, DOI: 10.1029/97GL03703 (1998).
[24]R. E. Ergun, D. Larson, R. P. Lin, J. P. McFadden, C. W. Carlson, K. A. Anderson, L. Muschietti, M. McCarthy, G. K. Parks, H. Reme, J. M. Bosqued, C. D'Uston, T. R. Sanderson, K. P. Wenzel, M. Kaiser, R. P. Lepping, S. D. Bale, P. Kellogg, and J.-L. Bougeret, Astrophys. J. **503**, 435 (1998).
[25]K. W. Ogilvie, L. F. Burlaga, D. J. Chronay, and R. Fitzenreiter, J. Geophys. Res. **104**, 22389, DOI: 10.1029/1999JA900294 (1999).
[26]C. Pagel, S. P. Gary, C. A. de Koning, R. M. Skoug, and J. T. Steinberg, J. Geophys. Res. **112**, A04103, DOI: 10.1029/2006JA011967 (2007).
[27]S. Saito and S. P. Gary, J. Geophys. Res. **112**, A06116, DOI: 10.1029/2006JA012216 (2007).
[28]J. D. Scudder and S. Olbert, J. Geophys. Res. **84**, 2755, DOI: 10.1029/JA084iA06p02755 (1979).
[29]J. D. Scudder and S. Olbert, J. Geophys. Res. **84**, 6603, DOI: 10.1029/JA084iA11p06603 (1979).
[30]M. V. Canullo, A. Costa, and C. F. Fontáin, Astrophys. J. **462**, 1005 (1996).
[31]Ø. Lie-Svendsen, V. H. Hansteen, and F. Leer, J. Geophys. Res. **102**, 4701, DOI: 10.1029/96JA03632 (1997).
[32]V. Pierrard, M. Maksimovic, and J. Lemaire, J. Geophys. Res. **104**, 17021, DOI: 10.1029/1999JA900169 (1999).
[33]V. Pierrard, M. Maksimovic, and J. Lemaire, Astrophys. Space Sci. **277**, 195 (2001).
[34]V. Pierrard, M. Maksimovic, and J. Lemaire, J. Geophys. Res. **106**, 29305, DOI: 10.1029/2001JA900133 (2001).
[35]S. Landi and F. G. E. Pantellini, Astron. Astrophys. **372**, 686 (2001).
[36]J. C. Dorelli and J. D. Scudder, J. Geophys. Res. **108**, 1294, DOI: 10.1029/2002JA009484 (2003).
[37]C. Vocks and G. Mann, Astrophys. J. **593**, 1134 (2003).
[38]C. Vocks, C. Salem, R. P. Lin, and G. Mann, Astrophys. J. **627**, 540 (2005).
[39]M. Maksimovic, I. Zouganelis, J.-Y. Chaufray, K. Issautier, E. E. Scime, J. E. Littleton, E. Marsch, D. J. McComas, C. Salem, R. P. Lin, and H. Elliott, J. Geophys. Res. **110**, A09104, DOI: 10.1029/2005JA011119 (2005).
[40]K. Appert, T. M. Tran, and J. Vaclavik, Phys. Rev. Lett. **37**, 502 (1976).
[41]O. Ishihara and A. Hirose, Phys. Rev. Lett. **46**, 771 (1981).
[42]O. Ishihara and A. Hirose, Phys. Fluids **26**, 100 (1983).
[43]O. Ishihara and A. Hirose, Phys. Fluids **26**, 1783 (1983).
[44]L. Muschietti, I. Roth, and G. Delory, J. Geophys. Res. **102**, 27217, DOI: 10.1029/97JA02532 (1997).
[45]P. H. Yoon, T. Rhee, and C.-M. Ryu, J. Geophys. Res. **111**, A09106, DOI: 10.1029/2006JA011681 (2006).
[46]C. T. Dum, Phys. Plasmas **1**, 1821 (1994).